Liu, Shubin; Ni, Hongjian; Wang, Xueying; Wang, Peng; Li, Ning

Article

Numerical study of the compound vertical and horizontal impact cutting with a single PDC cutter

Energy Reports

Provided in Cooperation with:
Elsevier

Suggested Citation: Liu, Shubin; Ni, Hongjian; Wang, Xueying; Wang, Peng; Li, Ning (2020) : Numerical study of the compound vertical and horizontal impact cutting with a single PDC cutter, Energy Reports, ISSN 2352-4847, Elsevier, Amsterdam, Vol. 6, pp. 1520-1527, https://doi.org/10.1016/j.egyr.2020.05.020

This Version is available at:
https://hdl.handle.net/10419/244141

Energy Reports 6 (2020) 1520–1527

Contents lists available at ScienceDirect

Energy Reports

journal homepage: www.elsevier.com/locate/egyr

Research paper

Numerical study of the compound vertical and horizontal impact cutting with a single PDC cutter

Liu Shubin [a], Ni Hongjian [a,*], Wang Xueying [a], Wang Peng [a], Li Ning [b]

[a] School of Petroleum Engineering, China University of Petroleum (East China), Qingdao 266580, PR China
[b] PetroChina Tarim Oilfield Company, Korla 841000, PR China

ARTICLE INFO

Article history:
Received 14 February 2020
Received in revised form 17 May 2020
Accepted 20 May 2020
Available online xxxx

Keywords:
Vertical impact
Horizontal impact
Cutting process
Failure mode
Cutting efficiency

ABSTRACT

Extensive studies have been carried out on vertical or horizontal impact cutting because they are both high-efficiency rock breaking methods, but little attention has been paid to impact cutting with simultaneous vertical and horizontal impact loads. In this work, we conducted numerical simulations to study the mechanism of compound vertical and horizontal impact (CVHI) cutting. Firstly, a finite element analysis model considering the strain rate effect was established, and the parameters of the rock were adjusted by fitting laboratory test data of granite. Then, the differences in the cutting process between conventional cutting and CHVI cutting were analyzed, and a series of simulations were conducted to research how the vertical impact load affects the cutting mode. Finally, other simulations were performed with different horizontal impact loads to reveal the reason for improving cutting efficiency. Due to the applied vertical impact load, the rock failure mode is transformed from the ductile mode into the brittle mode. Besides, the torsional impact load can speed up the cutting process by promoting the generation, propagation, and connection of cracks. Therefore, the cutting efficiency is significantly improved with the action of CVHI loads.

1. Introduction

Initially, hydraulic impactors, which direction of the impact force is mainly in axial, were developed to increase the drilling efficiency of roller bits (Graf and Kogan, 1972). This drilling method is suitable for drilling soft to hard strata. Compared with roller bits, PDC bits have the advantages of high drilling efficiency and long service life, and they are very suitable for use in homogeneous formations with hardness ranging from soft to medium-hard. However, attempts to drill hard rock in deep formations using PDC bits usually results in a poor rate of penetration (ROP) and bit footage. Therefore, researchers combined hydraulic impactors with PDC bits by refining the design of performance parameters (Powell et al., 2013). The amplitude is designed at a low level to reduce the damage, and the frequency is designed at a high level to adapt to high-speed rotation of PDC bits. On the other hand, PDC bits are made more and more firm to resist the damage from the impact forces, and researchers even developed special drill bits for impact drilling. In recent years, compound axial and torsional impact (CATI) drilling technology has been developed, and this technology has performed well in field applications, which can be seen in examples from Xu et al. (2016) and Liu et al. (2018). The research on rock-breaking mechanisms of CATI drilling is still very insufficient, which inevitably restricts the further promotion of this technology. Therefore, it is necessary to conduct related research.

In the research on conventional rock cutting with PDC bits, researchers have performed much work on laboratory experiments, theoretical analysis, and numerical simulations. Several analytical and empirical models, including those of Evans (1972), Nishimatsu (1972), Lebrun (1978) and Detournay and Defourny (1992), on conventional rock cutting have been proposed according to a metal cutting model proposed in Merchant's study (1945). The study by Adachi et al. (1996) demonstrated a linear relationship between the forces and the cutting depth of shallow cutting. However, when the cutting depth exceeds the critical value, the failure mode changes. Richard et al. (1998) proposed the combination of deep cutting and shallow cutting by separating the cutting mechanism into two different processes according to the cutting depth, which was validated by scratch test data. Jaime (2011) proposed that analytical models should be applied with caution depending upon the failure regime, which is primarily dominated by the depth of the cut. In the study by Jaime et al. (2015), simulation studies were performed using the finite element method to investigate rock failure mechanisms.

Studies (Khorshidian et al., 2012; Deen et al., 2011; Ostasevicius et al., 2010; Pavlovskaia et al., 2015) have proven that

* Corresponding author.
E-mail address: nihj@upc.edu.cn (Ni H.).

https://doi.org/10.1016/j.egyr.2020.05.020

impact drilling technology is an effective way to improve the ROP. Studies (Tang et al., 1996; Shockey et al., 1974) of rock fracture mechanics show that impact loads can accelerate the rate of crack growth, which is the crucial difference between an impact load and static load.

Generally, traditional impact-assisted drilling technology encompasses axial impact drilling and torsional impact drilling. Axial impact drilling technology can improve the cutting depth and generate sizeable cuttings (Dyskin, 1999; Wiercigroch, 1997; Li et al., 2001; Wang et al., 2018). When drilling in a hard formation, the torque increases rapidly with increasing cutting depth, leading to the buildup and release of torsional energy in the drill string, commonly known as a stick–slip vibration. Torsional impact drilling technology, which converts hydraulic energy to instantaneous torque impact, can reduce the tendency of stick–slip vibration and improve the efficiency of traditional rock cutting failure (Deen et al., 2011).

To reveal the rock breaking mechanism of CATI drilling, we study the rock cutting process, the cutting forces, and the cutting size. The structure of this study is as follows. First, a finite element analysis model considering the strain rate effect is introduced (Section 2). Then, the fragmentation process, the cutting volume, and the cutting force are analyzed in Section 3. In Section 3.1, we study the differences in the cutting process between conventional cutting and CHVI cutting, and we conducted a series of simulations to study how the vertical impact load affects the cutting mode. In Section 3.2, other simulations were conducted with different horizontal impact loads to study the reason for improving cutting efficiency. Finally, we summarize the concluding remarks and discuss future research directions in Section 4.

2. FEM modeling of a sharp cutter

2.1. Ductile and brittle rock failure mode

Richard et al.'s research (1998) shows that the rock failure mode is related to the cutting depth: a ductile failure mode occurs in a shallow cutting, while a brittle failure mode occurs in a deep cutting. In the ductile mode, the cutting volume is closely related to the geometric shape and motion trajectory of the cutters. However, in the brittle mode, the failure of the rock is related to the generation and growth of cracks. Therefore, the ductile mode of failure leads to small particle-like cuttings, but the brittle mode of failure often leads to large chunk-like cuttings (Fig. 1).

2.2. Important aspects of the modeling

Simulations were conducted by using LS-DYNA. On the basis of the CATI drilling, we established a cutting model with a single sharp cutter, as shown in Fig. 2. In the model, the axial and torsional impact forces are assumed as the vertical and horizontal impact forces, respectively.

(1) Model geometry

Only 1/2 of the rock sample and the cutter are modeled to reduce the calculation time, as shown in Fig. 3. The width, length, and height of the rock sample are 14 mm, 44 mm, and 20 mm. For the PDC cutter, the diameter and length are 13 mm and 20 mm, respectively, and the rake angle is fixed at 15°.

(2) Element size and type

We use the tetrahedral mesh for the rock sample, as shown in Fig. 4. A fine mesh with an average element size of 0.24 mm forms

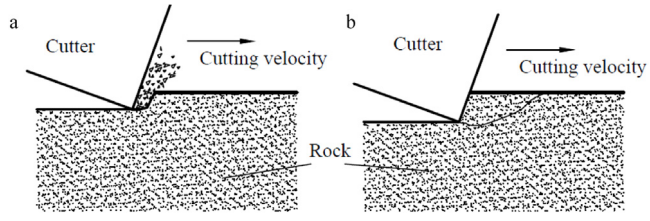

Fig. 1. Schematics of (a) shallow and (b) deep cutting.

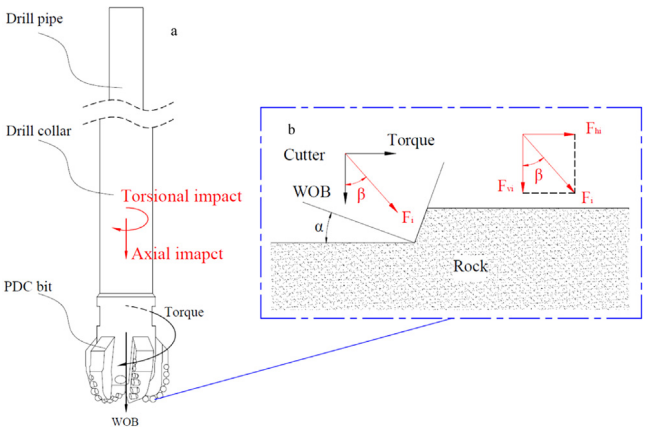

Fig. 2. Schematic of an analysis model with a sharp cutter: (a) a drilling model with compound axial and torsional impact loads; (b) the cutting model with an applied impact load (F_i). In the model, F_{vi} is the vertical impact load, F_{hi} is the horizontal impact load, β is the impact angle, and α is the rake angle of the cutter.

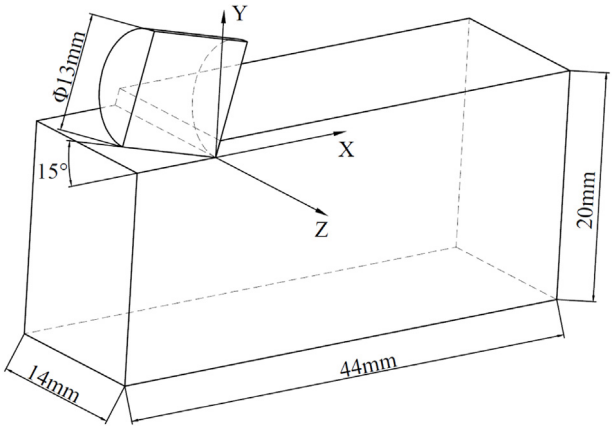

Fig. 3. A geometric model for conventional and CVHI cutting simulations. As for the rock model, the width, length, and height are 14 mm, 44 mm, and 20 mm. As for the cutter, the diameter and length are 13 mm and 20 mm, and the rake angle is 15°.

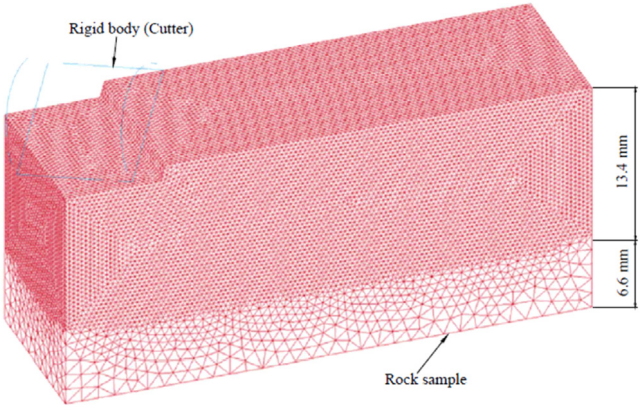

Fig. 4. FEM model for rock cutting with CVHI loads.

Table 1
Material properties of granite.

Poisson ratio	Mass density/kg·m^{-3}	Young's modulus/GPa	Uniaxial compressive strength/MPa
0.22	2878	58	165

the top 13.4 mm of the sample, while a coarse with an average element size of 1.2 mm was used for the bottom 6.6 mm of the sample. The total number of nodes and elements are 199,821 and 1,152,160, respectively.

(3) Boundary conditions

To simulate the infinite boundary of the actual stratum, we set the bottom, rear, left, and right surfaces as non-reflecting boundary surfaces. We also constrain all the degrees of freedom (DOFs) of the nodes on the bottom surface to fix the rock.

(4) Applied forces

In the conventional cutting simulation, the horizontal velocity of the cutter is 5 m/s, and the cutting depth is fixed at 1 mm. In the compound vertical and horizontal impact (CVHI) cutting simulation, the effects of axial impact force and torsional impact force on rock cutting are studied separately. As for the simulation of vertical impact load, the vertical impact forces are set as impact depths of 1.5 mm, 2 mm, 3 mm, and 4 mm, while the horizontal impact forces are all set as constant of 20 m/s. As for the study of horizontal impact load, the horizontal impact forces are set as velocities of 10 m/s, 20 m/s, 30 m/s, and 40 m/s, and the each of the runs has a constant impact depth of 4 mm.

(5) Material model

In this simulation, the deformation of the cutter is not taken into account, so we set the cutter as a rigid body. The continuous surface cap model (CSCM) is adopted to model the rock behavior. Jaime (2011) and Jaime et al. (2015) found that the CSCM works best among the models designed for rock cutting modeling, mainly due to its inclusion of element erosion and strain rate effect upon material failure.

2.3. Parameters of rock material

The CSCM encompasses the following key features (Murray et al., 2007; Murray, 2007): (a) isotropic constitutive equations, (b) three stress invariant yield surfaces, (c) a hardening cap that expands and contracts, (d) damage-based softening with erosion and modulus reduction, and (e) rate effects that are modeled with viscoplasticity. Below, we briefly recap the main points of model development.

The yield surface is formulated in terms of three stress invariants: j_1 is the first invariant of the stress tensor, j_2' is the second invariant of the deviatoric stress tensor, and j_3' is the third invariant of the deviatoric stress tensor. s_{ij}, s_{jk}, and s_{ki} are deviatoric stress tensors. P is pressure,

$$\begin{cases} j_1 = 3P \\ j_2' = \frac{1}{2}s_{ij}s_{ij} \\ j_3' = \frac{1}{3}s_{ij}s_{jk}s_{ki} \end{cases}. \tag{1}$$

The cap hardening parameter κ, is as follows:

$$f(j_1, j_2', j_3', \kappa) = j_2' - \Re^2 F_f^2 F_C, \tag{2}$$

where F_f is the shear failure surface, F_C is the hardening cap, and $\Re$ is the Rubin three-invariant reduction factor.

The shear surface F_f is defined along the compression meridian as

$$F_f(j_1) = \alpha - \lambda \exp^{-\beta j_1} + \theta j_1, \tag{3}$$

where the values of α, β, λ, and θ are selected by fitting the model surface to the strength measurements from a tri-axial compression test.

Concrete exhibits softening in the tensile and low to moderate compressive regimes,

$$\sigma_{ij}^d = (1-d)\sigma_{ij}^{vp}, \tag{4}$$

where d is a scalar damage parameter, σ_{ij}^{vp} is the stress tensor without damage, and σ_{ij}^d is the stress tensor with damage.

Damage initiates and accumulates when the strain-based energy terms exceed the damage threshold. Damage accumulation via the parameter d is as follows:

$$d = \begin{cases} \frac{0.999}{A}\left[\frac{1+A}{1+A\exp^{-C(\tau-r_0)}} - 1\right], & \tau > \tau_0, \\ 0, & otherwise \end{cases} \tag{5}$$

where A and C are two constants that control the softening shape and r_0 is the initial damage threshold when the rate effects are modeled via viscoplasticity.

$$r_0 = \left(1 + \frac{E\dot{\varepsilon}\eta}{r^S\sqrt{E}}\right) r^S. \tag{6}$$

Here, r^S is the damage threshold before the application of viscoplasticity. An element is under the intact condition when the parameter d is 0, and the parameter d increases under the action of the load until erosion occurs when the maximum value is 1.

The parameters of the CSCM were calibrated by granite uniaxial compression experiments. In the experiments, the diameter and height of the rock sample are 44 mm and 88 mm, respectively, and the other essential parameters are shown in Table 1. For the CSCM, the critical parameters are shown in Table 2. Fig. 5

Table 2
Key material parameters of the rock model.

Shear modulus G	Bulk modulus K	Tri-axial compression surface constant term α	Tri-axial compression surface linear term θ	Tri-axial compression surface nonlinear term λ	Tri-axial compression surface exponent β	Hardening initiation N_H	Hardening rate C_H
2.23×10^{10}	4.83×10^{10}	3.60×10^{7}	0.357485	9.05×10^{7}	1.93×10^{-8}	0	0
Ductile shape parameter B	Fracture energy in uniaxial stress G_{fc}	Brittle shape softening parameter D	Fracture energy in uniaxial tension G_{ft}	Fracture energy in pure shear stress G_{fs}	Shear-to-compression transition parameter *PWRC*	Shear-to tension transition parameter *PWRT*	Modify moderate pressure softening parameter *PMOD*
100	8995	0.001	89.95	89.95	5	1	0
Rate effects parameter for uniaxial compressive stress η_{0c}	Rate effects power for uniaxial compressive stress *NC*	Rate effects parameter for uniaxial tensile stress η_{0t}	Rate effects power for uniaxial tensile stress *NT*	Maximum overstress allowed in compression OVERC	Maximum overstress tension OVERT	Ratio of effective shear stress to tensile stress fluidity parameters STATE	Power which increases fracture energy with rate effects REPOW
0.0001	0.78	6.18×10^{-5}	0.48	3.28×10^{7}	3.28×10^{7}	1	1

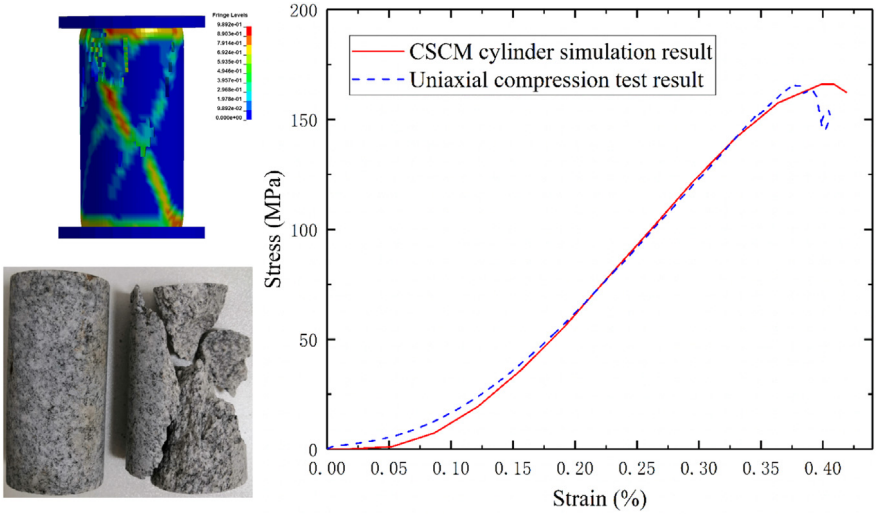

Fig. 5. A comparison of CSCM cylinder simulation and uniaxial compression test.

shows a comparison of the uniaxial compression test results with the numerical simulation results, and the results demonstrate that the CSCM model can well simulate the fragmentation and the stress–strain behavior of the rock.

Rate effects formulations are implemented to the model an increase in strength with increasing strain rate. The rate effects formulations are applied to the plasticity surface, the damage surface, and the fracture energy. The rate effects can be considered separately for three special stress states, namely the uniaxial tensile stress state, the uniaxial compressive stress state, and the pure shear stress state. For uniaxial compressive stress, the rate effect parameter, $\eta_{c0} = 1 \times 10^{-4}$, the rate effect power, $N_c = 0.78$, the maximum overstress allowed, $OVERC = 32.8 \times 10^{-3}$ GPa (2900 psi). For uniaxial tensile stress, the rate effect parameter, $\eta_{t0} = 6.18 \times 10^{-5}$, the rate effect power, $N_t = 0.48$, and the maximum overstress allowed, $OVERT = 32.8 \times 10^{-3}$ GPa (2900 psi), and the ratio of effective shear stress to tensile stress fluidity parameter, $S_{rate} = 1$.

3. Numerical simulations

3.1. The role of the vertical impact load in CVHI cutting

3.1.1. Cutting process

In Figs. 6 and 7, the color contours observed throughout the rock sample correspond to the cumulative element damage at a certain time. The element is in blue when the damage value is 0, and in red when the damage value is equal to or greater than 0.72. The creation of cracks in the simulations is expected when the red zone is propagated through the rock. Besides, an element fails once the damage value is greater than 0.99.

The simulation of the conventional cutting, which cutting depth is fixed at 1 mm, depicts the damage pattern at 4.59 ms, 6.3 ms, and 8.46 ms (Fig. 4). The results show that the failed elements of the rock mainly occurs around the cutter, and no cracks are propagated through the rock sample. The fragmentation patterns are consistent with the shallow cutting tests conducted by Richard et al. (1998). Therefore, the rock failure mode of the conventional cutting is a typical ductile mode. In the ductile failure mode, the rock fragmentation mechanism involves only the crushing of particles, and the fragmentation mainly occurs near the location where the rock surface is in contact with the cutter.

Different from the conventional cutting, the CVHI cutting can increase the cutting depth, which is critical to the transformation

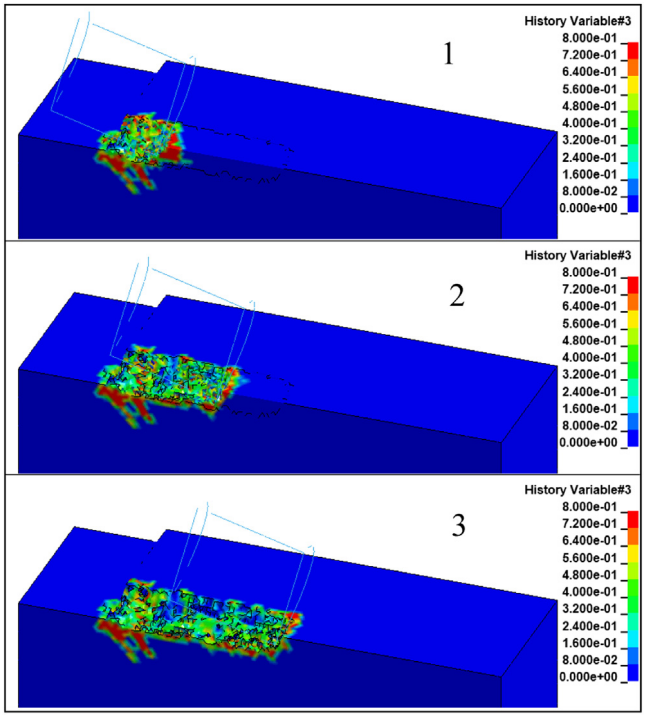

Fig. 6. Damage pattern for the conventional cutting. Simulation results at (1) t = 4.59 ms, (2) t = 6.30 ms, and (3) t = 8.46 ms.

of the rock failure mode. Hence, we simulated the cutting process of the different impact depths of 1.5 mm, 2 mm, 3 mm, and 4 mm. Besides, each simulation has the same initial cutting depth of 1 mm and the same horizontal impact load of 20 m/s.

Fig. 7 depicts the damage pattern for a sequence of three stages of the chip formation in the different runs. When the impact depth is 1.5 mm, the failed elements of rock are distributed around the cutter. However, when the impact depth is greater than 2 mm, the damage pattern showed some changes. Firstly, the failure of elements initiates from the corner at the tip of the cutter because the elements have fewer constraints than other elements, and the stress is highly concentrated (Fig. 7(b-1), (c-1), and (d-1)). Then, the cracks grow and propagate to the top surface of the rock, as shown in Fig. 7(b-2), (c-2), and (d-2). Finally, a chip

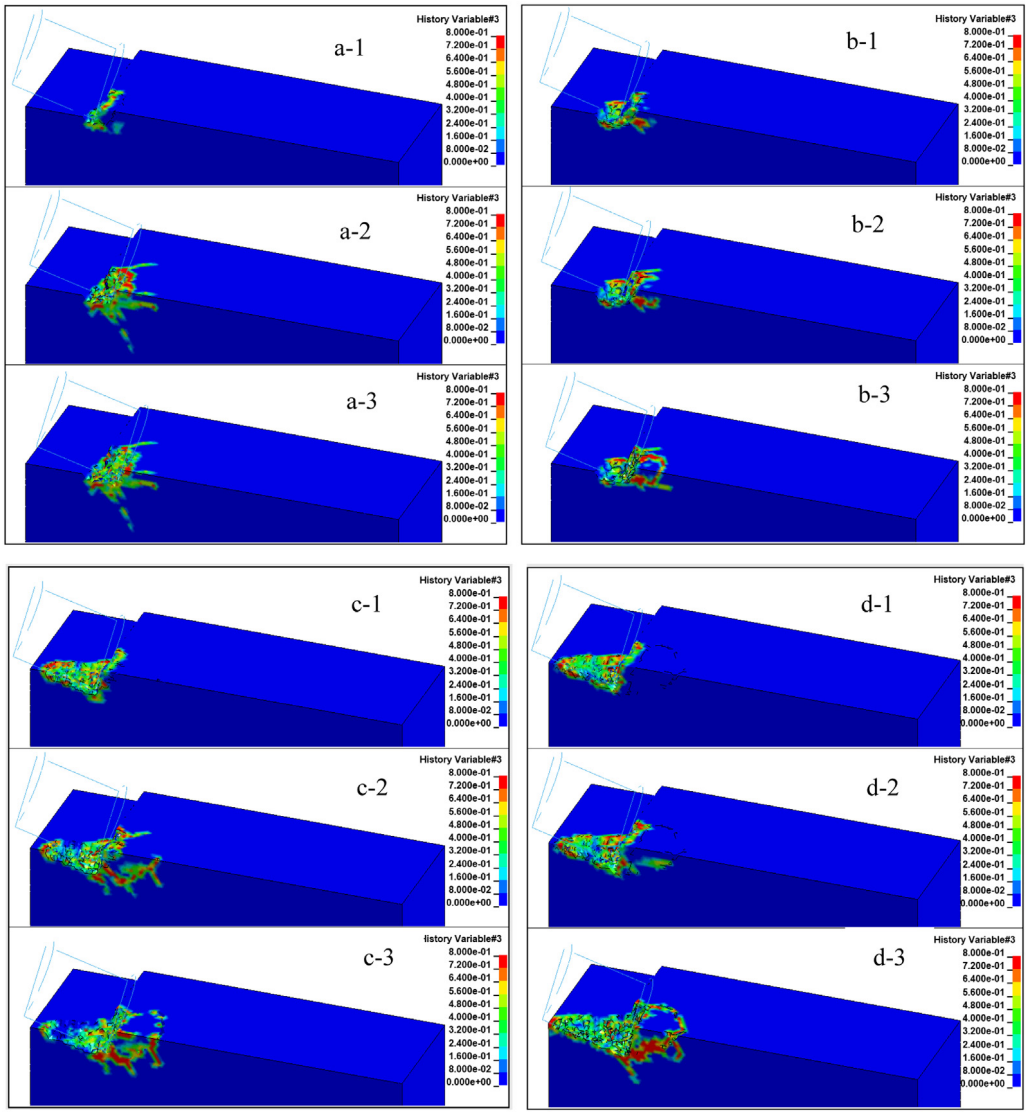

Fig. 7. Damage pattern for CHVI cutting. Simulation results at impact depth of (a) D = 1.5 mm, (b) D = 2 mm, (c) D = 3 mm. and (d) D = 4 mm.

is removed from the rock continuum piece, and the volume of the chip increases with the increase of impact depth, as illustrated in Fig. 7(b-3), (c-3), and (d-3).

The vertical impact can transform the mode of rock failure from the ductile into the brittle by increasing the cutting depth. For the conventional cutting, energy is dissipated mainly in the form of the broken-rock volume, so the cuttings are particle-like. For the CVHI cutting, damage accumulates through cracks, and energy is thus dissipated mainly in the form of a surface crack. Therefore the CVHI cutting leads to large chunk-like cuttings. However, it is important to note that the rock failure mode is still dominated by the ductile mode when the vertical impact depth is less than the threshold (1.5∼2 mm in this simulation).

3.1.2. Cutting volume

The cutting volume of the two failure modes is different: for the brittle failure mode, the cutting volume is related to the generation and growth of cracks; for the ductile failure mode, the cutting volume is related to the geometric of the cutter. Therefore, the projected volume and failed elements volume are both applied to the analysis of cutting volume.

The projected volume is the swept volume of the contact face of the cutter and rock. In the geometric model of the cutter (Fig. 8), the cutting depth $D = v_h t$, v_h is horizontal velocity of the cutter, R is the radius of cutter, and v is the resultant velocity, and θ is the angle of the resultant velocity.

The contact area (s) of the cutter at a certain time t can be expressed as:

$$s = 2\int_0^{z_t'} (D - y')dz' = 2\int_0^{\sqrt{2RD-D^2}} (v_h t - R + \sqrt{R^2 - z^2})dz'. \quad (7)$$

The projected volume ($V_{\mathrm{Pr}oj}$) at a certain time t is as follows:

$$V_{\mathrm{Pr}oj} = \int_0^t sv\cos(\frac{\pi}{2} - \alpha - \theta)dt, \quad (8)$$

where the v is the resultant velocity of the cutter.

Fig. 9 depicts the cutting volume of the conventional cutting simulation. The cutting volume increases linearly at 0.34∼0.36 ms, and it is approximately equal to the projected volume. Then, the damage accumulates over a larger zone in the rock sample, resulting in a rapid increase in the cutting volume. The slow and rapid growth of volume alternates in rock cutting, indicating a step evolution in rock fragmentation.

The results of different impact depths are shown in Fig. 10. Similar to the conventional cutting, there are two stages in the

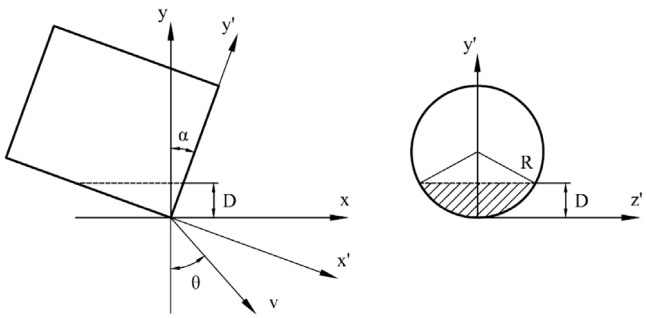

Fig. 8. The geometric model of the cutter. On the left, side view of the cutter; on the right, front view of the cutting face.

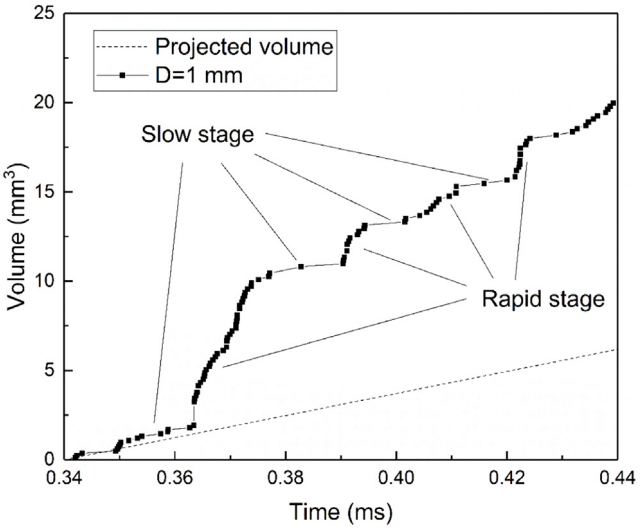

Fig. 9. The cutting volume of the conventional cutting, which cutting depth is fixed at 1 mm.

process of CVHI cutting: slow cutting stage and rapid cutting stage. In the slow stage, the actual volume is approximately equal to the projected volume. However, the curve deviates from the projected curve in the rapid stage because the chunk-like chip is removed from the rock in the rapid stage.

The results indicate that the deeper the impact depth, the larger the total volume. The cracks cannot be generated inside the rock in the shallow cutting because of the small damage zone. When the depth is greater than 2 mm, the cracks are originated and grow in the rock, resulting in a significant increase in the cutting volume.

3.1.3. Cutting force

Fig. 11 shows the cutting force history of CVHI cutting. The cutting forces increase in the slow stage and then decrease rapidly in the rapid stage. Intuitively, the impact depth has a strong influence on the amplitude and duration of the cutting force. In Fig. 11, the peak cutting forces are 555.1 N, 944.2 N, 1084.5 N, and 1317.5 N; the cutting time is 0.403 ms and 0.432 ms. 0.442 ms, and 0.458 ms. The results show that the amplitude of the cutting force in the simulation of a deep cutting is greater than that of a shallow cutting, and the duration of the force is longer in a deeper cutting.

In the drilling situation, when the cutting force is insufficient, the torque will build up through the deformation of the drilling strings until the cutting force exceeds the force required for rock breaking. This phenomenon is the so-called stick–slip, which can slow down the cutting process, resulting in low cutting efficiency. Hence, it is necessary to enhance the cutting force to mitigate the stick–slip.

3.2. The role of the horizontal impact load in CVHI cutting

Deep cutting depth with low applied cutting force can reduce the rate of cutting by inducing stick–slip, especially drilling in hard rock. It is an effective method to accelerate the cutting process by adding a horizontal impact load. To reveal the mechanism of cutting with different horizontal impact loads, we set the horizontal velocities as 5 m/s, 10 m/s, 20 m/s, 30 m/s and 40 m/s and the vertical impact depth are all as a constant of 4 mm.

Fig. 12 depicts the results of the cutting volume versus time. The percentage reduction, which defined as a percentage reduction of cutting time with no horizontal impact force (5 m/s) and different horizontal impact forces (10 m/s, 20 m/s, 30 m/s, and 40 m/s), are 7.8%, 17.8%, 21.2%, and 22.6%. Obviously, a higher horizontal impact load leads to a quicker fragmentation.

For the slow stage, the cutting time decrease with the horizontal velocity increase, which indicates that the effect of the horizontal impact on accelerating the rock fragmentation is weakening. Besides, because of the rate effect of the rock model, the amplitude of the cutting force increase with the horizontal velocity increase.

As a conclusion of the simulation study, the vertical impact load leads to an increase in the cutting depth, which is a crucial factor in the transition from a ductile mode to a brittle mode, and the horizontal impact load leads to the quick fragmentation. Therefore, a large cutting volume and high cutting efficiency are obtained with the combined effect of the vertical and horizontal impact loads.

4. Conclusions

The vertical impact force transforms the mode of rock failure from ductile into brittle by increasing the cutting depth. The cuttings are particle-like in the conventional cutting, while the CATI cutting leads to large chunk-like cuttings when the vertical impact depth exceeds the threshold (1.5∼2 mm in this simulation).

There are two stages in the process of CATI drilling: in the slow stage, the cutting volume is closely related to the geometric shape and motion trajectory of the cutters; in the rapid stage, the actual volume is related to the generation and growth of cracks.

A higher torsional impact load leads to a quicker fragmentation. Compared with cutting time with no horizontal impact force, the percentage reduction of cutting time with the impact force range from 7.8 to 22.6%.

It is an effective method to accelerate the cutting process by adding a torsional impact force. With the combined vertical and horizontal impact forces, drilling operators can obtain high drilling efficiency in drilling hard rock.

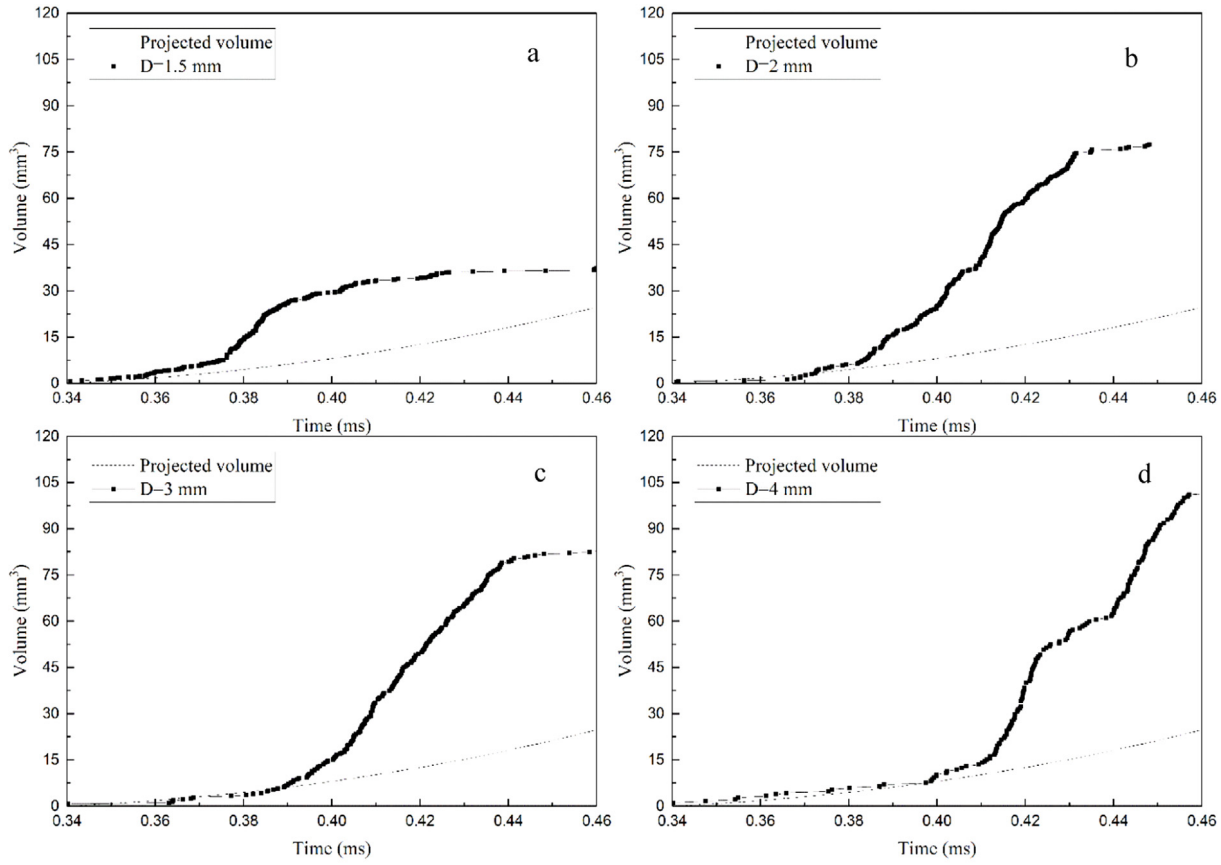

Fig. 10. A comparison of cutting volume with different impact depths. The impact depths are (a) 1.5 mm, (b) 2 mm, (c) 3 mm, and (d) 4 mm.

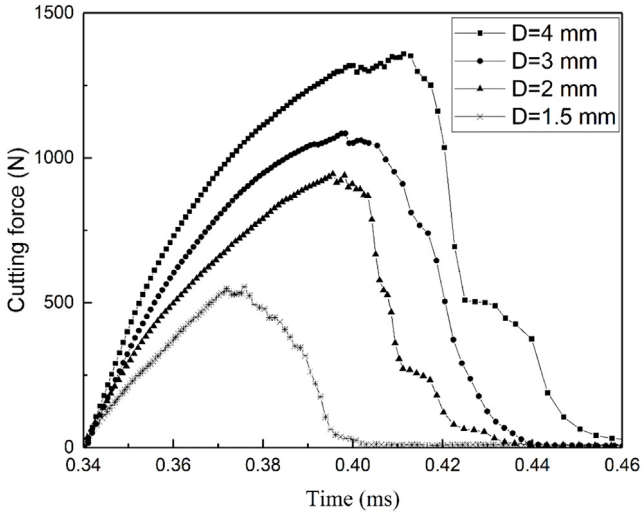

Fig. 11. Cutting forces for different impact depths of 1.5 mm, 2 mm, 3 mm, and 4 mm.

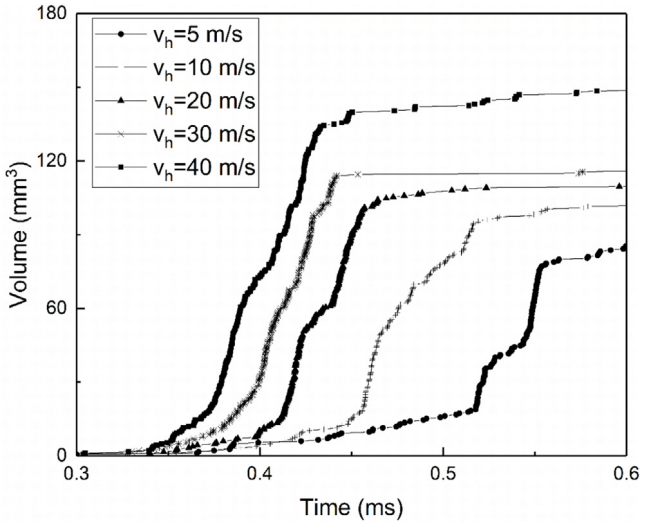

Fig. 12. Cutting volume for different horizontal velocities of 5 m/s, 10 m/s, 20 m/s, 30 m/s, and 40 m/s.

We believe the present study lays a foundation for further development. Based on the present research, we have developed a multi-direction impact drilling test device and a compound axial and torsional impact drilling tool. Studies of optimal impact parameters and field applications will be conducted in future work.

CRediT authorship contribution statement

Liu Shubin: Conceptualization, Methodology, Software. **Ni Hongjian:** Conceptualization, Methodology. **Wang Xueying:** Data curation, Writing - review & editing. **Wang Peng:** Writing - review & editing. **Li Ning:** Supervision, Formal analysis.

Declaration of competing interest

The authors declare that they have no known competing financial interests or personal relationships that could have appeared to influence the work reported in this paper.

Acknowledgments

The authors gratefully acknowledge the financial support of the National Natural Science Foundation of China (Grant No. 51704323), and financial support from Science and Technology Major Project of the China National Petroleum Corporation (No. ZD2019-183-005).

References

Adachi, J.I., Detournay, E., Drescher, A., 1996. Determination of rock strength parameters from cutting tests. Proc. NARMS 1517–1523.

Deen, C.A., Wedel, R.J., Nayan, A., et al., 2011. Application of a torsional impact hammer to improve drilling efficiency. In: SPE Annual Technical Conference and Exhibition. Society of Petroleum Engineers.

Detournay, E., Defourny, P., 1992. A phenomenological model for the drilling action of drag bits. Int. J. Rock Mech. Min. Sci. Geomech. Abstr. 29 (1), 13–23, Pergamon.

Dyskin, A.V., 1999. On the role of stress fluctuations in brittle fracture. Int. J. Fract. 100 (1), 29–53.

Evans, I., 1972. Line spacing of picks for effective cutting. Int. J. Rock Mech. Min. Sci. Geomech. Abstr. 9 (3), 355–361, Pergamon.

Graf, L.E., Kogan, D.I., 1972. Hydro-percussion machines and tools. Nedra, Moscow, Russia.

Jaime, M.C., 2011. Numerical Modeling of Rock Cutting and its Associated Fragmentation Process using the Finite Element Method. University of Pittsburgh.

Jaime, M.C., Zhou, Y., Lin, J.S., et al., 2015. Finite element modeling of rock cutting and its fragmentation process. Int. J. Rock Mech. Min. Sci. 80, 137–146.

Khorshidian, H., Mozaffari, M., Butt, S.D., 2012. The role of natural vibrations in penetration mechanism of a single PDC cutter. In: 46th US Rock Mechanics/Geomechanics Symposium. American Rock Mechanics Association.

Lebrun, M., 1978. Etude Théorique Et Expérimentale de L'Abattage Mécanique: Application à la Conception de Machines D'Abattage Et de Creusement. École Nationale Supérieure des Mines de Paris.

Li, X.B., Summers, D.A., Rupert, G., et al., 2001. Experimental investigation on the breakage of hard rock by the PDC cutters with combined action modes. Tunn. Undergr. Space Technol. 16 (2), 107–114.

Liu, S., Ni, H., Wang, X., et al., 2018. Rock-breaking mechanism study of axial and torsional impact hammer and its application in deep wells. In: IADC/SPE Asia Pacific Drilling Technology Conference and Exhibition. Society of Petroleum Engineers.

Merchant, M.E., 1945. Mechanics of the metal cutting process. I. Orthogonal cutting and a type 2 chip. J. Appl. Phys. 16 (5), 267–275.

Murray, Y.D., 2007. Users Manual for LS-DYNA Concrete Material Model 159. Federal Highway Administration. Office of Research, Development, and Technology, United States.

Murray, Y.D., Abu-Odeh, A.Y., Bligh, R.P., 2007. Evaluation of LS-DYNA Concrete Material Model 159. Federal Highway Administration. Office of Research, Development, and Technology, United States.

Nishimatsu, Y., 1972. The mechanics of rock cutting. Int. J. Rock Mech. Min. Sci. Geomech. Abstr. 9 (2), 261–270, Pergamon.

Ostasevicius, V., Gaidys, R., Rimkeviciene, J., et al., 2010. An approach based on tool mode control for surface roughness reduction in high-frequency vibration cutting. J. Sound Vib. 329 (23), 4866–4879.

Pavlovskaia, E., Hendry, D.C., Wiercigroch, M., 2015. Modelling of high frequency vibro-impact drilling. Int. J. Mech. Sci. 91, 110–119.

Powell, S.W., Herrington, D., Botton, B., et al., 2013. Fluid hammer increases PDC performance through axial and torsional energy at the bit. In: SPE Annual Technical Conference and Exhibition. Society of Petroleum Engineers.

Richard, T., Detournay, E., Drescher, A., et al., 1998. The scratch test as a means to measure strength of sedimentary rocks. In: SPE/ISRM Rock Mechanics in Petroleum Engineering. Society of Petroleum Engineers.

Shockey, D.A., Curran, D.R., Seaman, L., et al., 1974. Fragmentation of rock under dynamic loads. Int. J. Rock Mech. Min. Sci. Geomech. Abstr. 11 (8), 303–317, Pergamon.

Tang, C.Y., Tai, W.H., Lee, W.B., 1996. Modeling of damage behaviors of high impact polystyrene. Eng. Fract. Mech. 55 (4), 583–591.

Wang, P., Ni, H., Wang, R., 2018. A novel vibration drilling tool used for reducing friction and improve the penetration rate of petroleum drilling. J. Pet. Sci. Eng. 165, 436–443.

Wiercigroch, M., 1997. Chaotic vibration of a simple model of the machine tool-cutting process system.

Xu, Z., Jin, Y., Hou, B., et al., 2016. Rock breaking model under dynamic load with the application of torsional and axial percussion hammer. In: International Petroleum Technology Conference. International Petroleum Technology Conference.